Research Article | Vol. 26, No. 6 | 19 Mar 2018 | OPTICS EXPRESS 6771
Optics EXPRESS

Few-femtosecond extreme-ultraviolet pulses fully reconstructed by a ptychographic technique

MATTEO LUCCHINI,[1,2,*] GIACINTO D LUCARELLI,[1] MARIO MURARI,[1,2] ANDREA TRABATTONI,[3] NICOLA FABRIS,[4,5] FABIO FRASSETTO,[4] SANDRO DE SILVESTRI,[1,2] LUCA POLETTO,[4] AND MAURO NISOLI[1,2]

[1]*Department of Physics, Politecnico di Milano, 20133 Milano, Italy*
[2]*Institute for Photonics and Nanotechnologies, IFN-CNR, 20133 Milano, Italy*
[3]*Center for Free-Electron Laser Science (CFEL), DESY, 22607 Hamburg, Germany*
[4]*Institute for Photonics and Nanotechnologies, IFN-CNR, 35131 Padova, Italy*
[5]*Department of Information Engineering, University of Padova, 35131 Padova, Italy*
[*]*matteo.lucchini@polimi.it*

Abstract: Sub-10-fs pulses tunable in the extreme-ultraviolet (XUV) spectral region are particularly important in many research fields: from atomic and molecular spectroscopy to the study of relaxation processes in solids and transition phase processes, from holography to free-electron laser injection. A crucial prerequisite for all applications is the accurate measurement of the temporal characteristics of these pulses. To fulfill this purpose, many phase retrieval algorithms have been successfully applied to reconstruct XUV attosecond pulses. Nevertheless, their extension to XUV femtosecond pulses is not trivial and has never been investigated/reported so far. We demonstrate that ultrashort XUV pulses, produced by high-order harmonic generation, spectrally filtered by a time-delay compensated monochromator, can be fully characterized, in terms of temporal intensity and phase, by employing the ptychographic reconstruction technique while other common reconstruction algorithms fail. This allows us to report on the generation and complete temporal characterization of XUV pulses with duration down to 5 fs, which constitute the shortest XUV pulse ever achieved via a time-delay compensated monochromator.

OCIS codes: (320.0320) Ultrafast optics; (320.2250) Femtosecond phenomena; (320.7100) Ultrafast measurements.

References and links

1. F. Krausz and M. Ivanov, "Attosecond physics," Rev. Mod. Phys. **81**, 163–234 (2009).
2. F. Calegari, G. Sansone, S. Stagira, C. Vozzi and M. Nisoli, "Advances in attosecond science," J. Phys. B At. Mol. Opt. Phys **49**, 062001 (2016).
3. N. Nisoli, P. Decleva, F. Calegari, A. Palacios and F. Martín, "Attosecond Electron Dynamics in Molecules," Chem. Rev. **117**, 10760–10825 (2017).
4. A. Rundquist, C. G. Dufree, Z. Chang, C. Herne, S. Backus, M. M. Murnane and H.C. Kapteyn, "Phase-Matched Generation of Coherent Soft X-rays," Science **280**, 1412–1425 (1998).
5. Ch. Spielmann, N. H. Burnett, S. Sartania, R. Koppitsch, M. Schnürer, C. Kan, M. Lenzner, P. Wobrauschek and F. Krausz, "Generation of Coherent X-rays in the Water Window Using 5-Femtosecond Laser Pulses," Science **278**, 661–664 (1997).
6. L. Poletto, P. Villoresi, E. Benedetti, F. Ferrari, S. Stagira, G. Sansone and M. Nisoli, "Intense femtosecond extreme ultraviolet pulses by using a time-delay-compensated monochromator," Opt. Lett. **117**, 2897–2899 (2007).
7. J. K. Freericks, H. R. Krishnamurthy and Th. Pruschke, "Theoretical Description of Time-Resolved Photoemission Spectroscopy: Application to Pump-Probe Experiments," Phys. Rev. Lett. **102**, 136401 (2009).
8. B. Frietsch, R. Carley, K. Döbrich, C. Gahl, M. Teichmann, O. Schwarzkopf, Ph. Wernet and M. Weinelt, "A high-order harmonic generation apparatus for time- and angle-resolved photoelectron spectroscopy," Rev. Sci. Instrum. **84**, 075106 (2013).
9. M. Eckstein, C. Yang, F. Frassetto, L. Poletto, G. Sansone, M. J.J. Vrakking and O. Kornilov, "Direct Imaging of Transient Fano Resonances in N_2 Using Time-, Energy-, and Angular-Resolved Photoelectron Spectroscopy," Phys. Rev. Lett. **116**, 163003 (2016).

#318344 https://doi.org/10.1364/OE.26.006771
Journal © 2018 Received 22 Dec 2017; revised 9 Feb 2018; accepted 9 Feb 2018; published 6 Mar 2018

Optics EXPRESS

10. B. Erk, R. Boll, S. Trippel, D. Anielski, L. Foucar, B. Rudek, S. W. Epp, R. Coffee, S. Carron, S. Schorb, K. R. Ferguson, M. Swiggers, J. D. Bozek, M. Simon, T. Marchenko, J. Küpper, I. Schlichting, J. Ullrich, C. Bostedt, D. Rolles, A. Rudenko, "Imaging charge transfer in iodomethane upon x-ray photoabsorption," Science **345**, 288–291 (2014).
11. J. Schnadt, P. A. Brühwiler, L. Patthey, J. N. O'Shea, S. Sodergren, M. Odelius, R. Ahuja, O. Karis, M. Bassler, P. Persson, H. Siegbahn, S. Lunell, N. Martensson, "Experimental evidence for sub-3-fs charge transfer from an aromatic adsorbate to a semiconductor," Nature **418**, 620–623 (2002).
12. A. Ludwig, E. Liberatore, J. Herrmann, L. Kasmi, P. López-Tarifa, L. Gallmann, U. Rothlisberger, U. Keller and M. Lucchini, "Ultrafast Relaxation Dynamics of the Ethylene Cation $C_2H_4^+$," J. Phys. Chem. Lett. **7**, 1901–1906 (2016).
13. Y. Pertot, C. Schmidt, M. Matthews, A. Chauvet, M. Huppert, V. Svoboda, A. von Conta, A. Tehlar, D. Baykusheva, J. Wolf and H. J. Wörner, "Time-resolved x-ray absorption spectroscopy with a water window high-harmonic source," Science **355**, 264–267 (2017).
14. M. Eckstein, C. Yang, M. Kubin, F. Frassetto, L. Poletto, H Ritze, M. J.J. Vrakking and O. Kornilov, "Dynamics of N_2 Dissociation upon Inner-Valence Ionization by Wavelength-Selected XUV Pulses," J. Phys. Chem. Lett. **6**, 419–425 (2015).
15. Y. Mairesse and F.Quéré, "Frequency-resolved optical gating for complete reconstruction of attosecond bursts," Phys. Rev. A **71**, 011401 (2005).
16. M. Sabbar, S. Heuser, R. Boge, M. Lucchini, T. Carette, E. Lindroth, L. Gallmann, C. Cirelli, U. Keller, "Resonance Effects in Photoemission Time Delays," Phys. Rev. Lett. **115**, 133001 (2015).
17. M. Sabbar, S. Heuser, R. Boge, M. Lucchini, T. Carette, E. Lindroth, L. Gallmann, C. Cirelli, U. Keller, "Erratum: Resonance Effects in Photoemission Time Delays [Phys. Rev. Lett. 115, 133001 (2015)]," Phys. Rev. Lett. **119**, 219901 (2017).
18. J. Gagnon, Y. S. Yakovlev, "The direct evaluation of attosecond chirp from a streaking measurement," Appl. Phys. B **103**, 303–309 (2011).
19. M. Lucchini, A. Ludwig, L. Kasmi, L. Gallmann and and U. Keller, "Semi-classical approach to compute RABBITT traces in multi-dimensional complex field distributions," Opt. Express **23**, 8867–8879 (2015).
20. P.M. Paul, E.S. Toma, P. Breger, G. Mullot, F. Augé, Ph. Balcou, H.G. Muller and P. Agostini, "Observation of a Train of Attosecond Pulses from High Harmonic Generation," Science **292**, 1689–1692 (2001).
21. H. G. Muller, "Reconstruction of attosecond harmonic beating by interference of two-photon transitions," Appl. Phys. B **74**, s17-s21 (2002).
22. L. Cattaneo, J. Vos, M. Lucchini, L. Gallmann, C. Cirelli and U. Keller, "Comparison of attosecond streaking and RABBITT," Opt. Express **25**, 29060–29076 (2016).
23. A. Bouhal, R. Evans, G. Grillon, A. Mysyrowicz, P. Breger, P. Agostini, R. C. Constantinescu, H. G. Muller, and D. von der Linde, "Cross-correlation measurement of femtosecond noncollinear high-order harmonics," J. Opt. Soc. Am. B **14**, 950—956 (1997).
24. M. Kitzler, N. Milosevic, A. Scrinzi, F. Krausz and T. Brabec, "Quantum theory of attosecond XUV pulse measurement by laser dressed photoionization," Phys. Rev. Lett. **88**, 173904 (2002).
25. D. J. Kane, "Recent progress toward real-time measurement of ultrashort laser pulses," IEEE J. Quantum Electron. **35**, 421–431 (1999).
26. J. Gagnon, E. Goulielmakis and V. S. Yakovlev, "The accurate FROG characterization of attosecond pulses from streaking measurements," Appl. Phys. B **92**, 25–32 (2008).
27. M. Chini, S. Gilbertson, S. D. Khan and Z. Chang, "Characterizing ultrabroadband attosecond lasers," Opt. Express **18**, 13006–13016 (2010).
28. D. Spangenberg, E. Rohwer, M. H. Brügmann, and T. Feurer, "Ptychographic ultrafast pulse reconstruction," Opt. Lett. **40**, 1002–1005 (2015).
29. M. Lucchini, M. H. Brügmann, A. Ludwig, L. Gallmann, U. Keller and T. Feurer, "Ptychographic reconstruction of attosecond pulses," Opt. Express **23**, 29502–29513 (2015).
30. P. Sidorenko, O. Lahav, Z. Avnat, and Oren Cohen,"Ptychographic reconstruction algorithm for frequency-resolved optical gating: super-resolution and supreme robustness," Optica **2**, 1320–1330 (2016).
31. T. Witting, D. Greening, D. Walke, P. Matia-Hernando, T. Barillot, J. P. Marangos, and J. W. G. Tisch, "Time-domain ptychography of over-octave-spanning laser pulses in the single-cycle regime," Opt. Lett. **41**, 4218–4221 (2016).
32. J. Hyyti, E. Escoto, G. Steinmeyer, and T. Witting, "Interferometric time-domain ptychography for ultrafast pulse characterization," Opt. Lett. **42**, 2185–2188 (2017).
33. G.I. Haham, P. Sidorenko, O. Lahav, and O. Cohen, "Multiplexed FROG," Opt. Express **25**, 33007–33017 (2017).
34. M. Nisoli, S. De Silvestri and O. Svelto, "Generation of high energy 10 fs pulses by a new pulse compression technique," Appl. Phys. Lett. **68**, 2793–2795 (1996).
35. L. Poletto, P. Villoresi, F. Frassetto, F. Calegari, F. Ferrari, M. Lucchini, G. Sansone and M. Nisoli, "Time-delay compensated monochromator for the spectral selection of extreme-ultraviolet high-order laser harmonics," Rev. Sci. Instrum. **80**, 123109 (2009).
36. L. Poletto, F. Frassetto and P. Villoresi, "Ultrafast Grating Instruments in the Extreme Ultraviolet," IEEE J. Sel. Top. Quantum Electron. **18**, 467–478 (2012).
37. F. Frassetto, C. Cacho, C.A. Froud, I.C.E. Turcu, P. Villoresi, W.A. Bryan, E. Springate, and L. Poletto, "Single-grating monochromator for extreme-ultraviolet ultrashort pulses," Opt. Express **19**, 19169–19181 (2011).

Optics EXPRESS

38. J. Ojeda, C.A. Arrell, J. Grilj, F. Frassetto, L. Mewes, H. Zhang, F. van Mourik, L. Poletto, and M. Chergui, "Harmonium: A pulse preserving source of monochromatic extreme ultraviolet (30âĂŞ110âĂŁeV) radiation for ultrafast photoelectron spectroscopy of liquids," Struct. Dyn. **3**, 023602 (2016).
39. M. Ito, Y. Kataoka, T. Okamoto, M. Yamashita, and T. Sekikawa, "Spatiotemporal characterization of single-order high harmonic pulses from time-compensated toroidal-grating monochromator," Opt. Express **18**, 6071-6078 (2010).
40. H. Igarashi, A. Makida, M. Ito and T. Sekikawa, "Pulse compression of phase-matched high harmonic pulses from a time-delay compensated monochromator," Opt. Express **20**, 3725–3732 (2012).
41. F. Frassetto, P. Villoresi and L. Poletto, "Optical concept of a compressor for XUV pulses in the attosecond domain," Opt. Express **16**, 6652–6667 (2008).
42. M. Mero, F. Frassetto, P. Villoresi, L. Poletto and K. Varjú, "Compression methods for XUV attosecond pulses," Opt. Express **19**, 23420–23428 (2011).
43. T. E. Glover, R. W. Schoenlein, A. H. Chin and C. V. Shank, "Observation of Laser Assisted Photoelectric Effect and Femtosecond High Order Harmonic Radiation," Phys. Rev. Lett. **76**, 2468–2471 (1996).
44. K. W. DeLong, Rick Trebino, J. Hunter and W. E. White, "Frequency-resolved optical gating with the use of second-harmonic generation," J. Opt. Soc. Am. B **11**, 2206–2215 (1994).
45. R. Trebino, K. W. DeLong, D. N. Fittinghoff, J. N. Sweetser, M. A. Krumbugel, B. A. Richman and D. J. Kane, "Measuring ultrashort laser pulses in the time-frequency domain using frequency-resolved optical gating," Rev. Sci. Instrum. **68**, 3277-3295 (1997).
46. C. Iaconis and I.A. Walmsley, "Spectral phase interferometry for direct electric-field reconstruction of ultrashort optical pulses," Opt. Lett. **23**, 792–794 (1998).

1. Introduction

The process of high-order harmonic generation (HHG) in gas is at the center of active experimental and theoretical investigation since its discovery and it is at the heart of the emergence of attosecond science [1–3]. The ultrashort temporal duration is not the only interesting feature of harmonic radiation. As HHG can cover the spectral region from ultraviolet (UV) to soft X-rays [4, 5] in a table-top setup, the harmonic radiation can be used to perform a large variety of time-resolved experiments, without the need for big facilities like synchrotrons or free electron lasers. Moreover, even if the attosecond resolution is lost after the selection of a single harmonic, the radiation has potentially temporal duration of the order of few femtoseconds [6]. Therefore, it can find application in a wide range of research areas where a proper degree of energy resolution is preferred to an extreme temporal resolution. Remarkable examples are time- and angular-resolved photoemission spectroscopy (tr-ARPES) [7–9] or femtosecond pump-probe spectroscopy of core and deep valence levels [10–14]. For all these applications, a proper measurement of the temporal characteristics of the harmonic radiation is required. Due to the limited flux, one possibility is to combine the extreme-ultraviolet (XUV) radiation with a portion of the generating infrared (IR) pulse as it is done in the frequency-resolved optical gating for the complete reconstruction of attosecond bursts (FROG CRAB) technique [15]. While this technique has been extensively tested and investigated for isolated attosecond pulses, its extension to few-femtosecond XUV pulses is not trivial and still has to be proven. The narrower bandwidth associated with a single harmonic and the associated loss of sub-cycle resolution, reduce the level of information redundancy in a FROG CRAB trace. For this reason the most commonly used reconstruction algorithms cannot be easily applied to few-femtosecond XUV pulses. Here we show, both with numerical simulations and experimental data, that the reconstruction of the temporal amplitude and phase of single harmonics can be obtained with the FROG CRAB technique when combined with a robust iterative algorithm. In particular, we demonstrate that the ptychographic technique is a powerful method to achieve full reconstruction of the temporal characteristics of single harmonic pulses. The validation of this reconstruction method allowed us to report on the generation and temporal characterization of the shortest XUV pulses ever produced by the use of a time-delay compensated monochromator (TDCM) [6], with duration down to 5 fs.

The paper is organised as follows: in section 2 we present the key features of the FROG CRAB method applied to the measurement of the temporal characteristics of single harmonic pulses. In particular, we show that the chirp of the harmonic and IR pulses is directly imprinted in the

Optics EXPRESS

photoelectron spectrogram, obtained by ionizing a target gas with the XUV pulse in the presence of the IR pulse, as a function of the temporal delay between the two pulses. Section 3 proves that it is possible to retrieve the temporal characteristics of the radiation by using the ptychographic algorithm. In section 4 we report on the experimental application of this reconstruction method to XUV pulses spectrally selected by a TDCM. In the last section we present a simplified cross-correlation model, which intuitively explains the physical origin of the main features of the measured spectrograms.

2. Single harmonic spectrogram

FROG CRAB is the most commonly used method to characterize the temporal evolution of attosecond pulses. A single attosecond pulse (SAP) is used to ionize a rare gas. In absence of particular atomic structures or resonances [16, 17], the temporal properties of the XUV radiation are directly imprinted in the generated electron burst. A phase-locked IR pulse is then used to modulate the electron momenta before detection. By scanning the relative delay between IR and XUV pulses, a collection of streaked electron spectra is obtained, called spectrogram. While the center of mass of the spectrogram follows the opposite of the IR vector potential, $-A_{IR}(\tau)$, fingerprints of the SAP phase can be found in the electron yield distribution. For example, a quadratic term in the spectral phase of the SAP redistributes the electron spectral intensity giving an asymmetric streaking trace [18]. By applying suitable phase retrieval algorithms to the experimental spectrogram it is possible to obtain a precise temporal characterization of the SAP [15].

In the case of attosecond pulse trains, the spectrogram can be seen as a coherent superposition of SAP streaking traces [19]. As such, the collection of electron spectra is still sensitive to the XUV spectral phase. In this case, each harmonic will ionize the atom of the target gas giving an electron spectrum characterized by discrete peaks (main bands). When the IR field is simultaneously present, additional peaks, called sidebands (SBs), appear in between the harmonic peaks. They are produced by the absorption of a harmonic photon and the additional absorption or emission of an IR photon. The two indistinguishable pathways, produced by two adjacent harmonics, interfere and thus the SB signal oscillates with twice the IR frequency, ω_{IR} (see Fig. 1(a)). In case of relatively moderate IR peak intensities ($I_{IR} \sim 10^{11}$ W/cm^2), the SB signal can be analysed with the reconstruction of attosecond beating by two-photon transitions (RABBITT) method [20, 21], giving equivalent information and preserving the attosecond resolution without the need for iterative algorithms [22]. As the condition to apply RABBITT is the interference between different two-color ionization pathways, this technique can no longer be applied when a single high-order harmonic (HH) is selected from the comb. Therefore, the question remains how to properly extract the XUV and IR spectral phases from a single HH spectrogram and go beyond the simple cross-correlation approximation [23]. In the following we will provide an answer to this question and show that it is possible to temporally characterize single HHs by employing the FROG CRAB approach in combination with the ptychographic reconstruction technique.

In the strong field approximation (SFA), the spectrogram can be written as [24]:

$$S(p,\tau) = \left| \int dt E_{XUV}(t) d\left(p + A_{IR}(t-\tau)\right) e^{-i\phi(t-\tau)} e^{i\left(\frac{p^2}{2}+I_p\right)t} \right|^2, \tag{1}$$

where

$$\phi(t) = \int_t^{\infty} dt' \left(p A_{IR}(t') - \frac{A_{IR}^2(t')}{2} \right). \tag{2}$$

I_p is the target ionization potential, p is the electron momentum, τ is the relative delay between the XUV and the IR pulse, $E_{XUV}(t)$ is the harmonic electric field and d is the dipole transition matrix element.

Optics EXPRESS

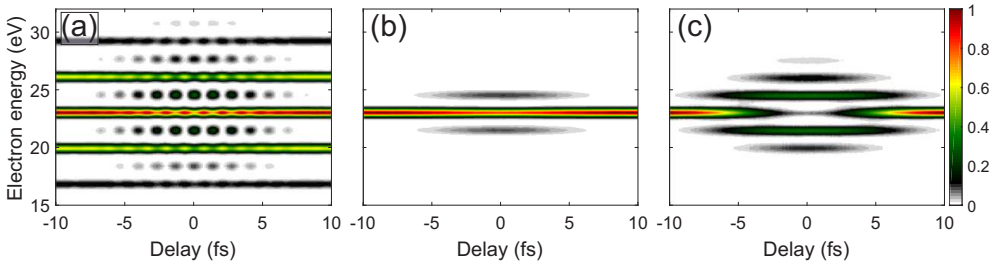

Fig. 1. (a) RABBITT-like spectrogram obtained with the full harmonic comb. (b), (c) Single harmonic spectrograms corresponding to HH25, calculated assuming $I_{IR} = 10^{11}$ and 10^{12} W/cm^2, respectively. Calculation parameters: temporal duration of each attosecond pulse in the train: 350 as; temporal duration of the APT: 5 fs; temporal duration of the IR pulse: $\tau_{IR} = 10$ fs. Both IR and XUV pulses are assumed to be transform limited. Ionization from Ar.

Figures 1(b) and 1(c) show how the simulated spectrogram changes after selection of a single harmonic: the spectrogram consists of a single emission peak corresponding to direct ionization via absorption of a XUV photon from the harmonic pulse. Additional peak pairs, spaced by $\hbar\omega_{IR}$ from the initial peak appear around zero time delay, produced by two-color ionization involving one XUV photon and at least one IR photon. As in the case of RABBITT, these peaks are called SBs and their number depends on the IR laser intensity, as shown in Fig. 1(c), which has been obtained by increasing the IR intensity from 10^{11} to 10^{12} W/cm^2. The spectral chirp of the IR

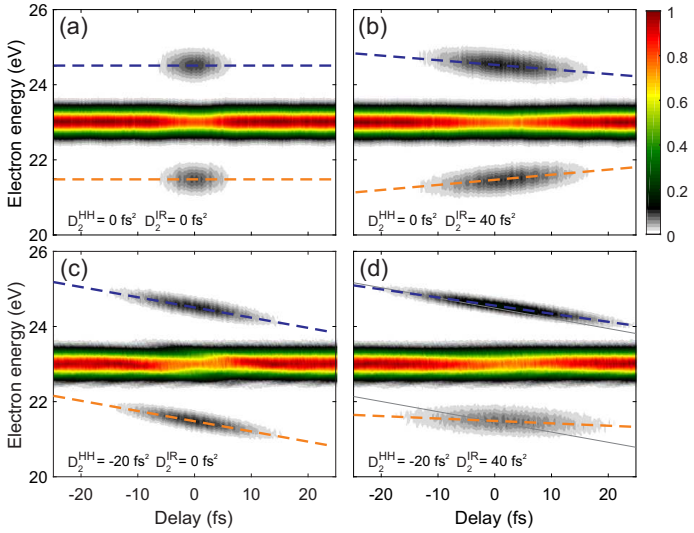

Fig. 2. Effect of the IR and XUV spectral chirp on the HH spectrogram. (a) Spectrogram of HH25 for transform limited (TL) radiation. Same spectrogram for TL XUV pulse and an IR chirp of 40 fs^2 (b), XUV chirp of -20 fs^2 and TL IR pulse (c), both XUV and IR chirped pulses with chirp of -20 fs^2 (d). The dashed blue and orange lines show the evolution of the SB center as a function of pump-probe delay. The thin grey lines in (d) show the tilt extracted from (c). Other calculation parameters: $\tau_{HH} = 5$ fs, $\tau_{IR} = 10$ fs, $I_{IR} = 10^{11}$ W/cm^2, ionization from Ar.

and XUV pulses notably affects the HH spectrogram, as displayed in Figure 2, where simulated

Optics EXPRESS

spectrograms for the same condition as in Fig. 1(b) are shown for different values of the linear chirp (quadratic phase) on both IR and XUV pulses. A chirp on the IR pulse produces tilted SBs with opposite angle, which thus assume a funnel shape (Fig. 2(b)). A chirp on the HH pulse gives also tilted SBs, but with the same tilt angle (Fig. 2(c)). As a result, the situation with both IR and XUV chirped pulses can reduce the tilt of one SB and preserve (or increase) the tilt of the other (Fig. 2(d)). This finding confirms that also in the case of single harmonic pulses the spectrogram is sensitive to the chirp of XUV and IR pulses. Therefore the basic requirements for the application of phase reconstruction algorithms are fulfilled. It is worth noticing that since with a single HH we lose sub-cycle resolution (typical of attosecond streaking) and since there are no interference effects (typical of RABBITT), the IR field does not need to be phase locked with the HH pulse, nor it is it necessary that the HH optical frequency is an integer multiple of the IR frequency.

3. Ptychographic reconstruction

The experimentally measured spectrogram $S(p, \tau)$ (see Eq. (1)) is a real and positive quantity so that phase informations are lost. So far, several algorithms have been proposed to reconstruct the phase associated with SAP spectrograms [25–27]. Among them the extended ptychographic iterative engine (ePIE) has proven to show superior degree of convergence and robustness [28, 29]. In contrast with the most commonly used algorithms based on principal projection component, in ePIE the delay and energy axis are not linked by a Fourier transform. This relaxes the need for data interpolation. Furthermore, the code is sensitive to the absolute value of the delay and not only to the relative step size, which results in an algorithm capable to work also with non equidistant sampling [30]. In addition, since ePIE cycles on each individual time delay step, one complete run over the spectrogram corresponds to several algorithm iterations making it robust to white noise and quick in convergence. These features make ptychography a perfect candidate for a variety of applications [31–33], like the extension of the FROG CRAB method to the reconstruction of single HH spectrograms. If compared to the results obtained with a full harmonic spectrum or a broad SAP spectrum, a HH spectrogram has a lower average density of non-zero points. For this reason convergence is more critical and conventional algorithms like the principal component generalized projection algorithm (PCGPA) and the least squared generalized projection algorithm (LSGPA) fail. Figure 3 shows the simulated and reconstructed spectrograms (Figs. 3, first row) of HH25 selected from a 7.5-fs comb. The first column displays the simulation while the second and third columns the reconstruction results obtained with PCGPA and LSGPA algorithms, respectively. Both algorithms fail in retrieving the correct IR pulse (second row) and reconstruct a XUV pulse which presents permanent SBs in its spectrum and strongly underestimated time duration (third and fourth row). In addition, even if we neglect the SBs in the harmonic spectrum, the algorithms do not reproduce the correct XUV spectral phase (compare the theoretical dashed grey curve in the last row of Fig. 3 with the dashed light blue and light green lines from PCGPA and LSGPA, respectively).

Also the application of standard ePIE algorithm can be critical. In particular with noisy experimental data or when a small delay window accompanied by a rough energy resolution are adopted. In order to guarantee reliable convergence without requiring a too high sampling (with consequent increase in calculation time) we modified the ePIE code. In particular, we added to each iteration: (1) a mobile average (smoothing) of the reconstructed XUV time phase and (2) an amplitude filter (super Gaussian). Without these precautions the algorithm will converge to an unphysical solution. In particular, the mobile average on the pulse phase is necessary to reduce the numerical high-frequency noise (with a time resolution of 207 as used in this work, we found that an average over two adjacent points is enough) while the filter (2) is used to set at zero the XUV field at the boundaries of the time window where numerical reflections can occur (in the simulation reported here a time window of 846.5 fs was used).

Optics EXPRESS

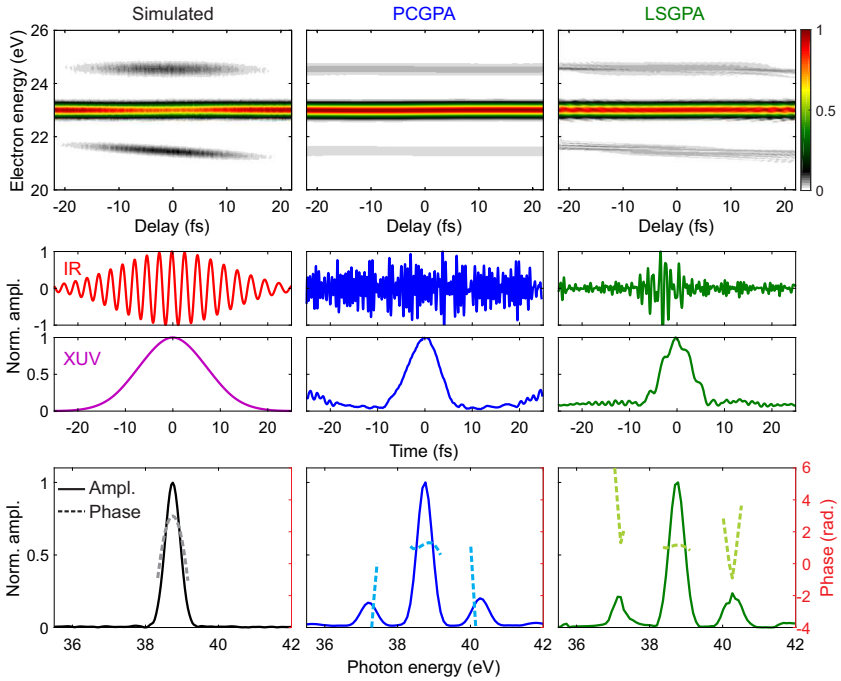

Fig. 3. Example of FROG-CRAB reconstruction with the PCGPA and LSGPA algorithms. The first column presents the simulation results using the same parameters as in the third row of Fig. 4: $\tau_{HH} = 7.5$ fs, $\tau_{IR} = 15$ fs, $D_2^{HH} = -20$ fs^2, $D_2^{IR} = -60$ fs^2, $I_{IR} = 10^{11}$ W/cm^2. From top to bottom the panels display: spectrogram, IR temporal behaviour (red curve), HH25 temporal profile (violet curve) and HH25 spectral amplitude (solid black curve) and phase (dashed grey curve). The second and third columns report the same quantities as retrieved by a PCGPA, LSGPA based FROG CRAB, respectively.

First we tested the convergence of ePIE applied to simulated spectrograms obtained by using Eq. (1). Figure 4 shows the calculation and reconstruction results for HH25 ionizing Ar atoms, using several different pulse parameters. The first two columns display the simulated and reconstructed spectrograms. The solid green and red curves in the third column represent the input XUV spectral amplitude and phase, respectively. The black and blue circles show the reconstruction results. The last column displays the input (solid red) and reconstructed (dashed light blue) IR pulse. The calculations in the first row have been performed in the case of transform-limited pulses, while in the second and third row we have considered chirped XUV and IR pulses. In particular, the second row shows the results in the case of a chirped XUV pulse with a group delay dispersion (GDD) $D_2^{HH} = -20$ fs^2 and a TL IR pulse. The third row displays the results calculated assuming that both XUV and IR pulses are chirped ($D_2^{HH} = -20$ fs^2, $D_2^{IR} = -60$ fs^2). The fourth row shows the results for the same parameters as the third, but with a ten times higher IR intensity. We note that the algorithm converges to the correct solution also when standard algorithms would fail (compare Fig. 3 and the third row in Fig. 4 which refers to the same pulse parameters). It is worth to point out that by selecting a single harmonic one loses sub-cycle resolution. Hence, the algorithm cannot reconstruct the carrier-envelope phase of the IR field. Nevertheless, the IR envelope and chirp were properly reconstructed in all the cases under examination (compare dashed light blue and solid red curves in the last column of Fig. 4). Therefore we can conclude that, starting from a HH spectrogram, ePIE can be used to reconstruct

Optics EXPRESS

the temporal duration and chirp of both XUV and IR pulses.

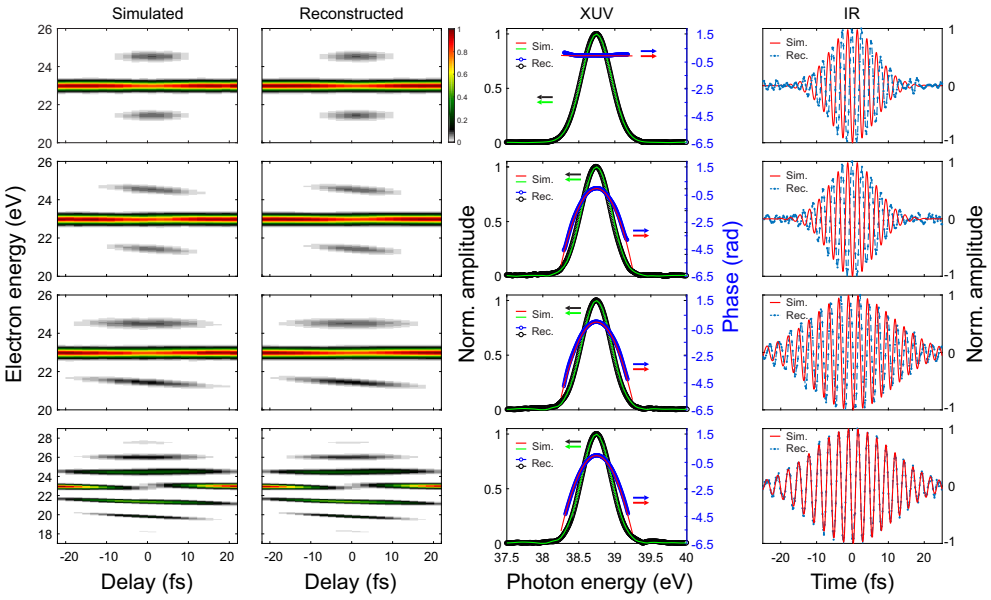

Fig. 4. Examples of ePIE reconstruction. The first two columns show the simulated and reconstructed spectrograms. The third column displays the simulated (solid lines) and reconstructed (circles) XUV spectral amplitude and phase. The last column on the right shows the simulated (solid red) and reconstructed (dashed light blue) IR electric field. The spectrogram in the first row is obtained with TL pulses. In the second row $D_2^{HH} = -20$ fs^2 and $D_2^{IR} = 0$ fs^2. In the third and fourth rows $D_2^{HH} = -20$ fs^2 and $D_2^{IR} = -60$ fs^2. For the first three rows the IR intensity is 10^{11} W/cm^2 while for the last row it is 10^{12} W/cm^2. The IR time duration is $\tau_{IR} = 15$ fs while the $\tau_{HH} = 7.5$ fs in all the simulations. The input traces are sampled with a delay step size of 2 fs and the reconstruction runs over 2000 iterations.

4. Experimental results

In the previous section we demonstrated with theoretical simulations that ePIE can correctly reconstruct the temporal properties of HHs. Here we want to prove that this method can, indeed, be applied to real experimental data. Few-cycle IR pulses were generated by a Ti-sapphire laser system delivering 25-fs pulses at 800 nm, energy of 1 mJ and repetition rate of 1 kHz. The pulses are further compressed down to $\sim 12-15$ fs and ~ 450-μJ pulse energy with a hollow-core fiber setup [34]. 80% of the beam is used to generate harmonics in a gas cell filled with Ar while the remaining 20% is suitably delayed and used as a probe. The harmonic radiation is then coupled into a TDCM [35]. In brief, the TDCM consists of two sections, each composed by two toroidal mirrors and one plane grating, working in a subtractive configuration to compensate for the temporal and spectral dispersion. As a result, it is possible to select a single harmonic, while preserving its original temporal duration [36]. Indeed, with monochromators based on a single-grating working in an off-plane geometry only XUV pulses with a time duration of few tens of fs have been reported so far [37, 38]. Comparable results in terms of time duration can be obtained with a TDCM [39], which further allows for the generation of shorter pulses, of the order of 10 fs [40] or less [6].

Optics EXPRESS

After the monochromator, XUV and IR pulses are recombined with a close-to-collinear geometry and focused into an interaction region equipped with a gas nozzle and a time-of-flight (TOF) spectrometer. The IR spatial profile in the focus has a FWHM of about 150 μm. After selection, the XUV beam size in the focus is < 50 μm and typical pulse energy is of the order of a few tens of pJ. Depending on the photon energy of the selected harmonic, Ar or Ne gas is ionized by the HH radiation. The photoelectron spectrum is then recorded by the TOF spectrometer. At the end of the beamline, a XUV photon spectrometer is used to characterise the spectral content of the harmonic radiation.

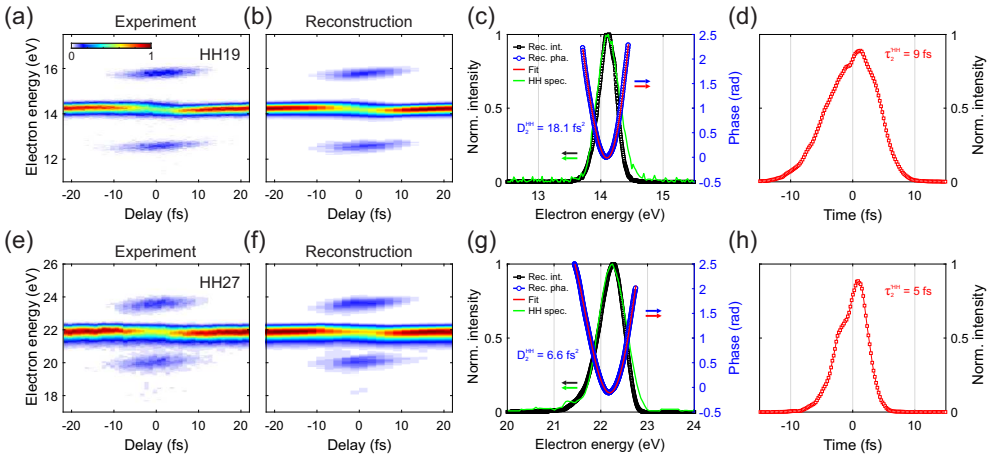

Fig. 5. Application of ePIE to experimental HH spectrograms. (a) Spectrogram of HH19 measured in Ar and scanning the pump-probe delay with a step of 1 fs. (b) ePIE reconstruction (2000 iterations with 2-fs delay step size as in Fig. 4). (c) Reconstructed spectral intensity (black squares) and phase (blue circles). The green solid line shows the harmonic photon spectrum as measured by the XUV spectrometer. The red solid curve represents the polynomial (5^{th} order) fit used to extract D_2^{HH}. (d) Corresponding harmonic intensity showing a duration below 10 fs. (e)-(h) Equivalent figures for HH27 ionizing Ne. Due to the smaller residual chirp, shorter XUV pulses can be obtained at higher frequencies.

The temporal response of the monochromator has been evaluated considering two effects on the ultrafast pulse given by the time-delay-compensating configuration. The first one is the compensation of the pulse-front tilt due to diffraction. This is accomplished when all the rays with equal wavelength emitted in different directions by the HH source travel the same optical path. Ideally the compensation is perfect for a double-grating configuration, although aberrations may give some residual distortions of the pulse-front, which has been evaluated via ray-tracing simulations to be below 2 fs. The second effect is the group delay dispersion introduced by the TDCM. Similarly to grating pulse shapers for the visible range, the TDCM can be considered as a XUV pulse shaper that introduces a controllable group delay dispersion [41, 42]. The optical path decreases linearly with the wavelength and this forces the GDD to be almost constant and positive. Given the parameters of the TDCM under examination, the GDD evaluated by ray-tracing simulations is found to be 20 fs^2 for HH19 and 7 fs^2 for HH27.

Figure 5 displays the experimental spectrogram and its ePIE reconstruction for HH19 (upper row) and HH27 (lower row). After only 2000 iterations of the algorithm the reconstructed spectrograms (Figs. 5(b) and 5(f)) show a very good agreement with the experimental ones. Further evidence for the correct convergence is given by the comparison between the harmonic spectrum measured with the XUV spectrometer (green curves in Figs. 5(c) and 5(g)) and the

Optics EXPRESS

reconstructed HH spectral distribution (black curves with square markers). The reconstructed IR pulses (not shown) have a temporal duration of 12 fs for the experiment in Fig. 5(a) and 15 fs for Fig. 5(e). These results are in good agreement with independent FROG measurements performed outside the evacuated lines, which gave a time duration of about 13 fs for both cases. As a rule of thumb, the duration of a single harmonic pulse is roughly equal to half the duration of the driving IR pulse. Therefore, we expect a XUV pulse duration of the order of 7 fs, if the TDCM is properly aligned. By repeating the reconstruction with different random initial guesses we found a pulse duration of 9 ± 0.5 fs for HH19 (Fig. 5(d)) and 5 ± 0.5 fs for HH27 (Fig. 5(h)), which represents, to the best of our knowledge, the shortest XUV femtosecond pulses ever measured at the output of a XUV monochromator. The residual parabolic chirp (see Figs. 5(c) and 5(g)) is mainly related to the group delay dispersion introduced by the TDCM. The resulting GDD is measured to be 18.1 ± 0.5 fs^2 for HH19 and 6.6 ± 0.5 fs^2 for HH27, in good agreement with the ray-tracing simulations.

5. Simple model

In this final section a simple model will be presented, which allows one to obtain a clear picture of the physical processes determining the main features of the HH spectrogram discussed in the previous sections. Furthermore, based on a cross-correlation picture, we will introduce a simple analytical expression that can be used to obtain a first rough estimation of the XUV pulse duration. Finally, we will compare the cross-correlation model [40, 43] with the ePIE reconstruction, discussing the advantages of the latter.

First we concentrate on the origin of the SB tilt. In case of transform limited XUV radiation and chirped IR pulses, the SB tilt can be easily understood in the photon picture as a mapping of the temporal distribution of the IR spectral content. At negative delays the IR pulse comes before the XUV pulse, hence the XUV pulse interacts mainly with the IR trailing edge. On the contrary, at positive delays the XUV pulse interacts with the IR leading edge. If the IR pulse is positively chirped, its instantaneous frequency increases with time, therefore at negative delays the SB signal will result from the absorption of a XUV photon and the absorption/emission of an additional IR photon of higher energy than the one seen at positive delays. A positive (negative) IR chirp thus gives a closing (opening) funnel in the HH spectrogram.

The situation is more complex in the case of chirped XUV pulses. If we assume that both IR and HH fields have a Gaussian temporal profile we can define them in frequency domain as:

$$\hat{E}_{HH}(\omega) = \frac{1}{2}\sqrt{2\pi}\sigma_{HH}e^{-\frac{\sigma_{HH}^2}{2}(\omega-\omega_{HH})^2}e^{-i\varphi_{HH}(\omega)} \tag{3}$$

$$\hat{E}_{IR}(\omega) = \frac{1}{2}\sqrt{2\pi}\sigma_{IR}E_0e^{-\frac{\sigma_{IR}^2}{2}(\omega-\omega_{IR})^2}e^{-i\varphi_{IR}(\omega)} \tag{4}$$

where E_0 is the IR field maximum amplitude and σ_j ($j = HH,\ IR$) is related to the full-width-half-maximum (FWHM) temporal durations, τ_j, of IR and XUV pulses by the following relation: $\tau_j = 2\sqrt{2\log(2)}\sigma_j$.

For the sake of simplicity, we limit the analysis to the case where the spectral phases, $\varphi_j(\omega)$, depend only quadratically with ω, i.e. $\varphi_j(\omega) = \frac{1}{2}D_2^j\omega^2$, where D_2^j represents the GDD coefficient. Let us consider moderate IR intensities, so that only one pair of SBs is formed. In this regime, the SB yield as a function of pump-probe delay, $SB(\omega,\tau)$, can be seen as a second order process that needs one IR photon and one XUV photon to ionize one electron. Following an approach similar to the one used for the second harmonic FROG we can write [44]:

$$SB(\omega,\tau) = \left|\int_{-\infty}^{\infty} E_{HH}(t)E_{IR}(t-\tau)e^{i\omega t}dt\right|^2, \tag{5}$$

Optics EXPRESS

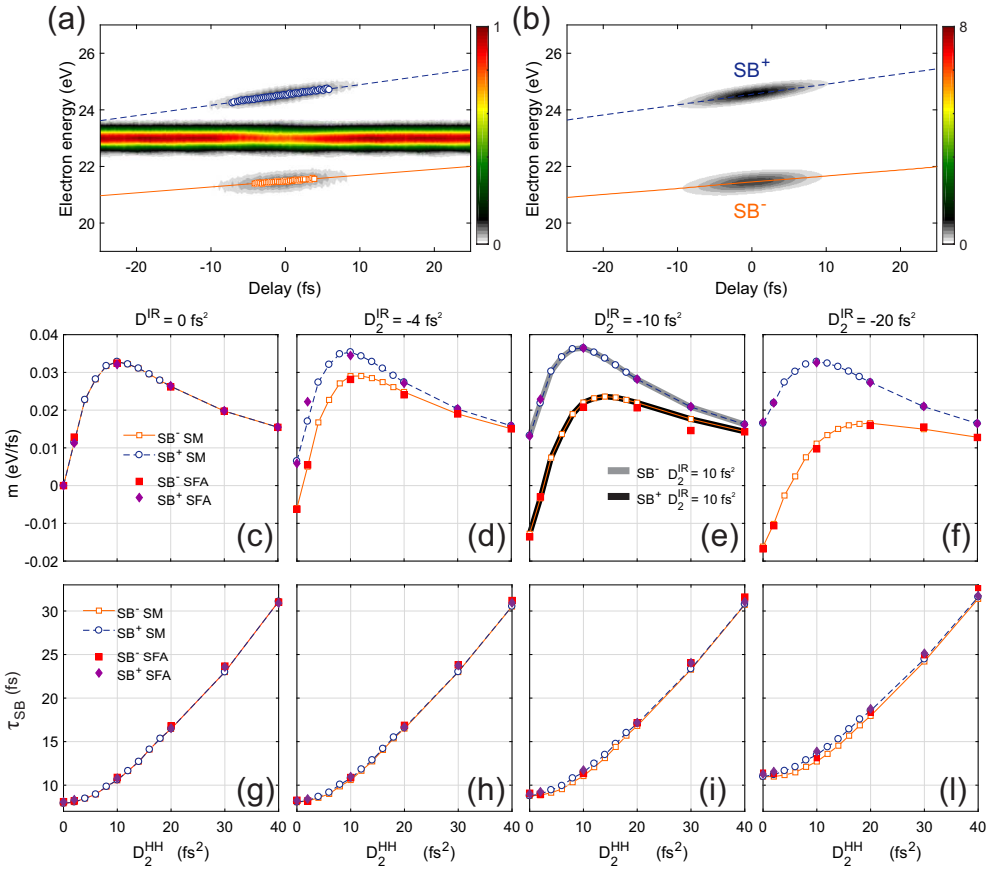

Fig. 6. Comparison between SFA and simple model. (a) HH spectrogram simulated with the SFA model of Eq. (1) for HH 25 in Ar. We have assumed: τ_{IR} = 10 fs, τ_{HH} = 5 fs, D_2^{HH} = 10 fs^2 and D_2^{IR} = −20 fs^2, I_{IR} = 10^{11} W/cm^2. (b) SB signal, $S(\omega,\tau)$, obtained with the simple model of Eq. (5) for the same parameters as in (a). (c)-(f) Upper (SB$^+$) and lower (SB$^-$) sideband tilt, m, extracted from the calculated spectrograms as a function of XUV chirp for D_2^{IR} equal to: (c) 0 fs^2, (d) −4 fs^2, (e) −10 fs^2, (f) −20 fs^2. In (e) the thicker lines show the tilt for an opposite IR chirp of 10 fs^2. (g)-(l), SB width corresponding to (c)-(f).

Optics EXPRESS

where $E_{HH}(t)$ and $E_{IR}(t)$ are the the temporal profiles obtained by inverse Fourier transform from Eqs. (3) and (4), respectively. Figure 6 shows a comparison between the spectrograms obtained by using Eq. (1) (Fig. 6(a)) and the simple model of Eq. (5) (Fig. 6(b)). Obviously this simplified model cannot reproduce the full HH spectrogram, but it can correctly predict the SB duration, τ_{SB} (defined as the FWHM of the Gaussian fit of the energy integrated SB signal), and tilt, m, with the advantage to be computationally much less demanding.

Equation (5) suggests that, depending on the relative time durations of the pulses, the SB signal can be seen as a time-gated Fourier transform of the XUV pulse or of the IR pulse. Therefore the SB tilt is expected to depend in a complex fashion on τ_j and D_2^j. Figures 6(c)-(f) show the evolution of the SB tilt, m, as a function of the XUV chirp, for different values of the IR chirp. Open markers identify the simple model (SM) results, while full markers refer to the SFA model: the two models are well in agreement. By comparing the values of m for the upper and lower SB at $D_2^{HH} = 0$ fs^2 through Figs. 6(c)-(f), one can observe that an increasing IR chirp leads to a monotonic opening (closing for $D_2^{IR} > 0$) of the funnel. On the other hand, m does not evolve monotonically with the XUV chirp. Moreover, the maximum value of m as a function of D_2^{HH} depends on both the IR and XUV time durations, as shown in Figs. 7(a) and 7(b). Even if it is possible to characterize the IR pulses separately, this suggests that it is not trivial to use the SB tilt extracted from the HH spectrogram to obtain a quick estimate of the XUV chirp. On the other hand, as shown in Figs. 6(g)-(l), τ_{SB} monotonically increases upon increasing the XUV chirp, with very small differences between the upper and lower SB (compare the results for SB$^+$ and SB$^-$ in the figure). Moreover, τ_{SB} increases monotonically also for an increasing IR chirp, independently from the SB under examination.

To understand the behaviour of τ_{SB} let's concentrate on the upper SB signal $SB^+(\tau)$ (equivalent reasoning can be done for the lower sideband $SB^-(\tau)$). If we use the complex notation for the fields, we can explicitly separate the field envelops, $E'_{HH}(t)$ and $E'_{IR}(t)$, from their carriers. Therefore we can rewrite Eq. (5) as follows:

$$SB(\omega,\tau) = \left| \int_{-\infty}^{\infty} E'_{HH}(t) E'_{IR}(t-\tau) e^{i(\omega-\omega^+)t} dt \right|^2, \tag{6}$$

where $\omega^+ = \omega_{HH} + \omega_{IR}$. If the pulse envelopes are long enough such that the phase term in the integral oscillates faster than the other terms we can write:

$$SB(\omega = \omega^+, \tau) = SB^+(\tau) = \left| \int_{-\infty}^{\infty} E'_{HH}(t) E'_{IR}(t-\tau) dt \right|^2. \tag{7}$$

Therefore, in the regime under examination, the energy integrated SB signal, $SB^+(\tau)$, can be seen as the cross correlation between the IR and XUV pulse envelopes. If $E'_{HH}(t)$ and $E'_{IR}(t)$ are Gaussians, $SB^+(\tau)$ will also have a Gaussian distribution with FWHM time duration $\tau_{SB} = \sqrt{\tau'^2_{HH} + \tau'^2_{IR}}$. By applying this simple relation to the experimental data of Figs. 5(a) and 5(e), it is possible to obtain a first rough estimation of the harmonic pulse duration of 8 fs and 6 fs in the case of HH19 and HH27, respectively. These values are in agreement with what obtained after ePIE reconstruction. Nevertheless, the simple cross-correlation formula is not always accurate. In particular, it fails in case of relatively short and chirped XUV pulses, as described here below.

It is known that for Gaussian pulses the HH and IR time durations, τ'_j, are linked to their transform limited time durations, τ_j, by the following relation:

$$\tau'_j = \tau_j \sqrt{1 + \left(8 \log(2) \frac{D_2^j}{\tau_j^2} \right)^2}. \tag{8}$$

Optics EXPRESS

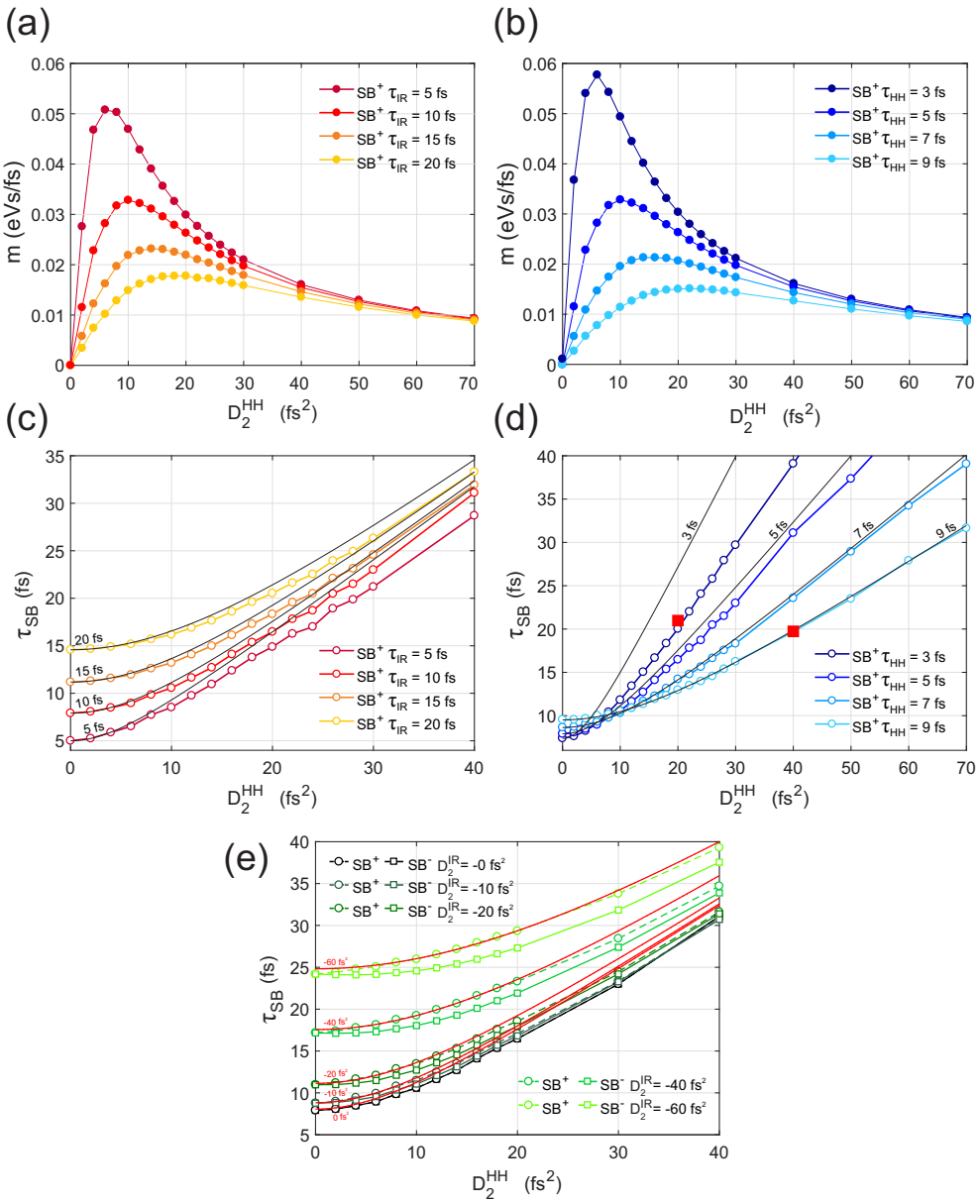

Fig. 7. Evolution of the SB tilt m and width τ_{SB} as a function of the pulse parameters as extracted from the simple model of Eq. (5). (a) m as a function of D_2^{HH} for different values of τ_{IR} (τ_{HH} = 5 fs and D_2^{IR} = 0). (b) m as a function of D_2^{HH} for different values of τ_{HH} (τ_{IR} = 10 fs and D_2^{IR} = 0). (c),(d) τ_{SB} as a function of D_2^{HH} for the same calculation parameters as in (a) and (b), respectively. (e) τ_{SB} as a function of D_2^{HH} for fix values of τ_{HH} = 5 fs and τ_{IR} = 10 fs, but different values of D_2^{IR}. In (c)-(e) the solid black and red curves with no markers show the SB width obtained with the cross-correlation formula of Eq. (8). $I_{IR} = 10^{11}$ W/cm^2 has been used in all the calculations. The red squares in (d) mark τ_{SB} reconstructed with ePIE for two showcases with short and long XUV TL time duration. As it is possible to observe ePIE correctly reconstructs τ_{SB} also when the cross-correlation formula fails (τ_{HH} = 3 fs).

Optics EXPRESS

Figures 7(a)-(d) display m and τ_{SB} for the upper SB, calculated with the simple model, as a function of D_2^{HH} for $D_2^{IR} = 0$ and different values of τ_{HH} and τ_{IR}. In Figs. 7 (c)-(d) we compare τ_{HH} extracted from the simple model (open coloured circles) with the prediction of the cross-correlation formula in Eq. (8) (black and red curves with no markers): there is a good agreement between the two models. In particular, the cross-correlation picture holds better for long XUV and IR pulses. For short IR pulses (~ 5 fs), the agreement is good only for relatively low GDD (compare the dark red curve with the black solid curve labelled with "5 fs" in Fig. 7(c)). The same is found while investigating different XUV pulse durations. In particular, for small values of τ_{HH} the HH bandwidth starts to be comparable to the energy separation between SB and main band. As a result one can observe fine interference structures in the spectral region where SB and main band overlap and thus the cross-correlation formula clearly fails to reproduce τ_{SB} (compare the dark blue curve and the black curve labelled with "3 fs" in Fig. 7(d)). In the case of chirped IR pulses, Fig. 7(e) shows that the analytical prediction (red solid curves labelled with the corresponding value of D_2^{IR}) agrees with the most tilted SB for which the sign of IR and XUV induced tilts is the same. This suggests that it is possible to use the SB duration τ_{SB} to estimate the XUV duration and chirp. By measuring the IR temporal profile with an independent technique (like FROG [45] or SPIDER [46]) and extracting τ_{SB} from the most tilted SB in the HH spectrogram one can employ the analytical cross-correlation expression to extract the actual HH time duration τ'_{HH}. Since the TL time duration τ_{HH} can be extracted by the inverse Fourier transform of the electron spectra at big negative (or positive) pump-probe delays, one can finally estimate the HH chirp by comparing τ_{HH} with τ'_{HH}, without the need for iterative algorithms.
We would like to stress that, even if computationally more demanding, the FROG CRAB reconstruction presents a series of advantages compare to the cross-correlation model. First, as the ePIE algorithm reconstructs both IR and XUV pulses, it does not require another independent measure of the IR field. Moreover, it works also with non-Gaussian pulses. Finally, it is not limited to long and weakly chirped pulses. The red square marks in Fig. 8(d) show the reconstructed τ_{SB} for 3-fs XUV pulses with $D_2^{HH} = 20$ fs^2 and 9-fs XUV pulses with $D_2^{HH} = 40$ fs^2. While both cross-correlation and ePIE manage to predict the right SB duration for the 9-fs pulses (giving a D_2^{HH} of 39.54 fs^2 and 40.39 ± 0.5 fs^2, respectively), only the ePIE matches the 3-fs pulse result. In particular, if one uses the cross-correlation based method described above to get the GDD coefficient, he will find $D_2^{HH} = 14.23$ fs^2 instead of 20 fs^2. A polynomial fit of the ePIE reconstructed spectral phase delivers a value of $D_2^{HH} = 20.2 \pm 0.5$ fs^2, in much better agreement with the theoretical input.

6. Conclusions

We have demonstrated that ultrashort XUV pulses produced by HHG and spectrally selected by a monochromator can be temporally characterized by using the FROG CRAB technique in combination with the extended ptychographic engine, where other standard reconstruction algorithm and the cross-correlation formula would fail. Since a proper temporal characterization of the light pulses is the prerequisite to improve the resolution of time resolved spectroscopy, our findings are relevant for a broad range of applications based on few-femtosecond XUV pulses. In addition, sub-10-fs pulses, tunable in the XUV, have been measured with pulse duration down to 5 fs around 29 nm. This constitutes, to the best of our knowledge, the shortest harmonic pulse ever measured, limited only by the current geometry of the optics employed. A further optimization could lead to even shorter pulses, suitable to investigate dynamics unfolding on very few fs (like spin diffusion, electron hopping, dynamical screening) which remain at the moment largely unexplored.